Synergistic and antagonistic effects of deterministic and stochastic cell-cell variations

Søren Vedel,[1,2,*] Andrej Košmrlj,[3,4] Harry Nunns,[2,5] and Ala Trusina[2,†]

[1]*Niels Bohr International Academy, Niels Bohr Institute, University of Copenhagen, Blegdamsvej 17, DK-2100 Copenhagen, Denmark*
[2]*Center for Models of Life, Niels Bohr Institute, University of Copenhagen, Blegdamsvej 17, DK-2100 Copenhagen, Denmark*
[3]*Department of Mechanical and Aerospace Engineering, Princeton University, Princeton, New Jersey 08544, USA*
[4]*Princeton Institute for the Science and Technology of Materials, Princeton University, Princeton, New Jersey 08544, USA*
[5]*Division of Biology and Biological Engineering, California Institute of Technology, 1200 E. California Boulevard, Pasadena, California 91125, USA*

(Received 10 February 2022; accepted 5 April 2024; published 9 May 2024)

By diversifying, cells in a clonal population can together overcome the limits of individuals. Diversity in single-cell growth rates allows the population to survive environmental stresses, such as antibiotics, and grow faster than the undiversified population. These functional cell-cell variations can arise stochastically, from noise in biochemical reactions, or deterministically, by asymmetrically distributing damaged components. While each of the mechanisms is well understood, the effect of the combined mechanisms is unclear. To evaluate the contribution of the deterministic component we developed a mathematical model by mapping the growing population to the Ising model. To analyze the combined effects of stochastic and deterministic contributions we introduced the analytical results of the Ising-mapping into an Euler–Lotka framework. Model results, confirmed by simulations and experimental data, show that deterministic cell-cell variations increase near-linearly with stress. As a consequence, we predict that the gain in population doubling time from cell-cell variations is primarily stochastic at low stress but may cross over to deterministic at higher stresses. Furthermore, we find that while the deterministic component minimizes population damage, stochastic variations antagonize this effect. Together our results may help identifying stress-tolerant pathogenic cells and thus inspire novel antibiotic strategies.

DOI: 10.1103/PhysRevE.109.054404

I. INTRODUCTION

Despite identical genetic makeup, cells in a population are never the same. This phenotypic diversity is functional and allows clonal populations to outperform individual cells. As an example, just variations in *Escherichia coli* doubling times alone have been found to be sufficient for a population to grow faster than individual cells, a phenomenon referred to as entropic gain [1]. Variations in doubling times are also beneficial for dealing with stresses—sudden changes in the environment, such as heat, antibiotics, etc., that disrupt cellular homeostasis by damaging proteins and DNA. Slowly growing cells tend to be more stress-resilient [2] and by diversifying into fast-growing stress-sensitive and slow-growing stress-tolerant cells [3] populations can both grow fast in a stress-free environment and survive sudden stresses. Other well-established functional outcomes of phenotypic diversity include improved multicellular migration [4] and functional roles in gene circuits [5].

The phenotypic diversity in single-cell growth rates is commonly attributed to stochastic fluctuations in protein numbers [1,6] or metabolism [7]. However, recent findings indicate the presence of a deterministic component as well: Cells can diversify through a process known as asymmetric damage segregation (ADS) [Fig. 1(a)] [4,8,9]. In this process, at cell division, the damaged proteins of a mother cell are split asymmetrically between the two daughter cells. The damaged proteins are functionally impaired due to misfolding or aggregation caused by external stressors, such as heat shock, antibiotics, or oxidative conditions. The accumulation of damaged proteins leads to slower physiological processes, including cell growth. Given that cells with a higher burden of damaged proteins grow slower [10–15], the primary consequence of ADS is that the differences in damaged proteins in two sister cells result in different growth rates. The difference in growth rates between sister cells is further amplified at every division along the lineages that consistently avoid or inherit the damage [illustrated for *E. coli* bacteria by the green-shaded and top lineage in Fig. 1(a), respectively]. Between these extremes lie the lineages with all the other combinations of damage inheritance. Thus, ADS generates a structured population tree with correlated lineages [Fig. 1(a)] while increasing the population growth and decreasing the mean damage in the population [8,16,17]. ADS is a general phenomenon [18,19] across cell types and organisms from bacteria [10,20] to more complex organisms such as yeasts [9,11] and mammalian cells [21–24] including neuronal stem cells [25].

Under physiological conditions cells experience both random and deterministic effects [1,8]. However, it remains unclear how the stochastic and deterministic components interact and together contribute to population fitness. Do the

*svedel@nbi.dk
†trusina@nbi.dk

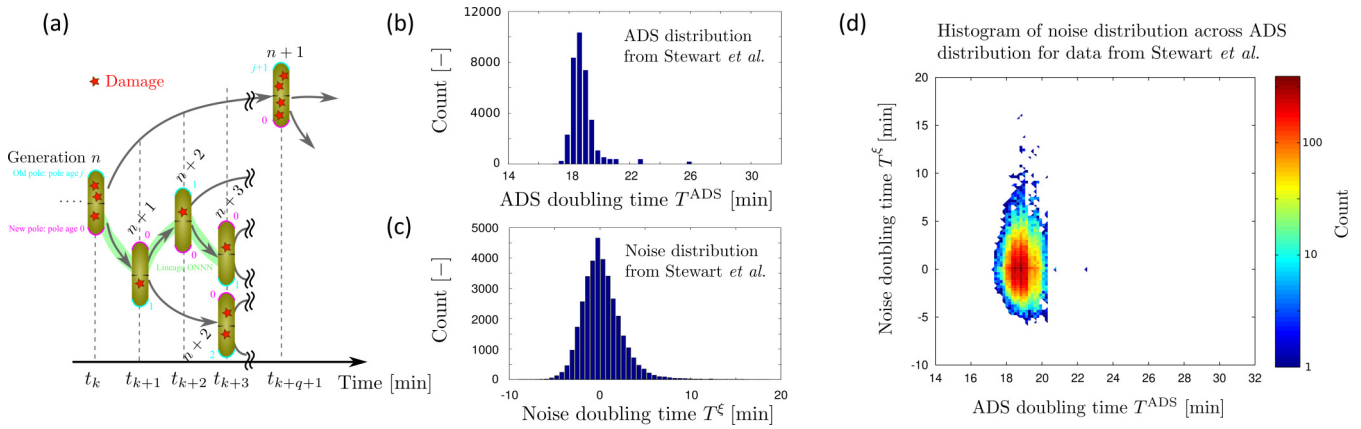

FIG. 1. (a) Schematic illustration of damage redistribution in a population of dividing cells. The doubling time T of the cell is slowed down by the accumulated damage [10,16] [Eq. (2)], and all cells acquire environmental damage (each red star in the schematic corresponds to λ amount of damage). At division, the damage is inherited asymmetrically resulting in different doubling times in the two sisters [Eq. (3)]. Green shading marks the lineage starting from an old cell of age j where cells consequently evade damage, i.e., the lineage $\ell = \mathrm{ONNN}$. (Model parameters in the schematic: $a = 1$, $t_{\min} = 0$, $\mu\lambda = 1$). (b), (c) The distribution of ADS doubling times (b) and noise [variations from average doubling time (c)] extracted via noise-filtering [Eq. (1)]. (d) Histogram of noise distribution around ADS distribution based on a grid of $(N_{\mathrm{ADS}}, N_{\xi}) = (100, 100)$ bins using the data from Stewart *et al.* [10] illustrates the absence of statistical dependence between noise and ADS.

two sources of diversity interact positively by adding together or perhaps even amplifying the effects of each other? Or do they antagonize each other? In addition to their conceptual importance, answering these questions could help identifying slow-growing stress-tolerant cells and thus inspire novel antibiotic strategies.

In pursuing these general questions with application across cell types, we used *E. coli* as a model system. Leveraging methods developed for our previous study [16], we combined published experimental data on ∼40 000 cells, theoretical modeling developed here and numerical simulations, and arrived at three novel results. First, we find that despite noise dominating the experimental distribution of the cells' doubling times, the contributions from ADS and noise are statistically independent, so that the diversity from ADS creates a "scaffold" on top of which the diversity from random noise is added. Second, we show that the deterministic contribution from ADS can be described analytically by mapping the growing population of cells to the Ising model [26,27]. Analytical results, confirmed by simulations and experimental data, suggest the nearly linear relationship between population diversity and stress. Furthermore, assuming that the coefficient of variation for stochastic component does not increase with stress, we predict that the entropic gain crosses over from stochastic at low stress to deterministic at higher stresses. Third, we find that while stochastic and deterministic effects *add together* in reducing population doubling time, they *antagonize* each other in reducing population damage levels.

II. RESULTS

A. Experimental data analysis finds statistical independence of ADS and noise

Previous experimental analyses have found that the doubling times of *E. coli* cells exhibit significant stochastic variations in doubling times in addition to the deterministic variations introduced by ADS [8,10,13,15,16]. To analyze the combined, stochastic and deterministic, effects we first sought to understand the relationship between ADS and non-ADS diversity, and to that end, we re-analysed experimental data by Stewart *et al.* [10] and our own previously published experiments [16] together covering 40 thousand individual cells from 144 colonies (details of all experimental datasets provided in Table I).

The rod-shaped *E. coli* divide along the middle by inserting new cell wall, resulting in a so-called old pole (existing cell end) and new pole in each new sister cell. It has been found that ADS localizes protein damage (misfolded proteins) at the old pole [14,15]. The propensity for damage accumulation at a given old pole increases with the *pole age*—the number of cell divisions that particular pole has participated in.

Because only a fraction of the mother cell's accumulated damage is inherited by the old pole at each division [13,15], a series of consecutive damage evasion events (consecutive new-poles) is required for full cellular rejuvenation. Conversely, in the old pole, the impact of damage is compounded over time as newly damaged proteins are added to the existing pool by ADS. In other words, since the amount of accumulated damage determines the reduction in single-cell growth rate, the order of inheritance influences the contribution of ADS to the cell's doubling time.

We used this understanding to separate the stochastic contributions of noise from the deterministic contribution of ADS by grouping cells with the same full lineage history ℓ, e.g., $\ell = \mathrm{ONNN}$ for the lineage highlighted in green in Fig. 1(a) where O and N correspond to the inherited old and new pole, respectively. We took the median doubling time of each group as an estimate of the ADS contribution to the doubling time of cell i from group ℓ, $T^{\mathrm{ADS}}_{\ell,i}$ [Fig. 1(e)]. The variation in doubling times within a group is caused by an *ADS-independent*

TABLE I. Overview of experimental data used and results for χ^2 contingency table tests of statistical independence between ADS and noise distributions for all experimental conditions. The listed P value is the probability of finding a similar or worse χ^2 statistic under the null hypothesis that the two distributions are statistically independent. For all tests we have used $(N_{\mathrm{ADS}}, N_\xi) = (100, 100)$ for 9801 degrees of freedom [DOF $= (N_{\mathrm{ADS}} - 1)(N_\xi - 1)$]. The 0.95 confidence level for this χ^2-distribution is 1.0032×10^4. Mutant MC4100Δ*clpB* cells were engineered with *ClpB-YFP* on plasmids activated by lacI^q. KM = kanamycin, an antibiotic.

Experiment	Source	Cell type	No. of cells	Stress	χ^2	P value
Stewart *et al.*	Ref. [10]	MG1655	35,049	UV, low	7.965×10^3	1
Mutant 37 °C	Ref. [16]	MC4100Δ*clpB*	1756	Heat, low	2.873×10^3	1
Mutant 42 °C	Ref. [16]	MC4100Δ*clpB*	1704	Heat, medium	2.851×10^3	1
Mutant 37 °C with 0.5 μg/mL KM	Ref. [16]	MC4100Δ*clpB*	1804	Antibiotic, medium	2.517×10^3	1
WT 37 °C	Ref. [16]	MC4100	2090	Heat, low	3.720×10^3	1
WT 42 °C	Ref. [16]	MC4100	2084	Heat, medium	4.267×10^3	1
WT 37 °C with 0.5 μg/μl KM	Ref. [16]	MC4100	1948	Antibiotic, medium	3.491×10^3	1

stochastic noise $T^{\xi}_{\ell,i}$, such that the doubling time of cell i from group ℓ, $T_{\ell,i}$ can be represented as a sum of deterministic and stochastic components:

$$T_{\ell,i} = T^{\mathrm{ADS}}_{\ell,i} + T^{\xi}_{\ell,i}. \tag{1}$$

This method for separating stochastic and ADS effects is a more accurate extension of our previously published method [16] since it bins cells based on the entire lineage history as opposed to only the last two generations. The origins of the noise $T^{\xi}_{\ell,i}$ could be time-additive noise (randomness in cell division machinery) [1], noisy single-cell growth rates (e.g., due to noisy gene expression [28]) and a range of possible cell-size control mechanisms leading to variations in cellular lifetimes [29–33]. No matter the source, the noise can be modeled by the functional form of Eq. (1) under appropriate considerations; see Supplemental Material [44] Sec. S1 for details.

We used the method to extract the distributions of doubling times for ADS and noise T^{ADS}, T^{ξ}. For illustration, in Fig. 1 we show the results from the dataset by Stewart *et al.* In line with previous reports [8], we observe that the distribution of T^{ADS} [Fig. 1(b)] is more narrow than the noise distribution T^{ξ} [Fig. 1(c)].

To understand their combined effects on populations, we then analyzed whether the distributions of ADS and noise exhibited any significant correlation. For this, we used a χ^2 contingency table to test for statistical independence between T^{ADS} and T^{ξ}, with the null hypothesis that the distributions are statistically independent. To perform the test we binned each of the distributions of $f_{\mathrm{ADS}}(T^{\mathrm{ADS}})$ and $f_{\xi}(T_{\xi})$ into N_{ADS} and N_ξ bins, resulting in a $N_{\mathrm{ADS}} \times N_\xi$ table of the number of noise counts (individual cells) $\mathcal{N}_{i,j}$ per ADS bin i and noise bin j, and the number of ADS counts per ADS bin $\sum_j \mathcal{N}_{i,j}$ [Fig. 1(d) illustrates the table for the data of Stewart *et al.*]. Assuming that noise is independent of ADS, the number of cells in each entry i, j in the $N_{\mathrm{ADS}} \times N_\xi$ table should be given by the relative amount of cells per ADS bin i, $p_i = \sum_j \mathcal{N}_{i,j} / \sum_i \sum_j \mathcal{N}_{i,j}$, multiplied by the total number of noise cells for noise bin j, $\tilde{\mathcal{N}}_j = \sum_i \mathcal{N}_{i,j}$ (summed across all ADS bins i for noise bin j). Comparing these expected number of cells per entry in the $N_{\mathrm{ADS}} \times N_\xi$ table to the actually recorded number is then done via the statistic $Q = \sum_{i=1}^{N_{\mathrm{ADS}}} \sum_{j=1}^{N_\xi} (\mathrm{observed}_{i,j} - \mathrm{expected}_{i,j})^2 / \mathrm{expected}_{i,j} = \sum_{i=1}^{N_{\mathrm{ADS}}} \sum_{j=1}^{N_\xi} (\mathcal{N}_{i,j} - p_i \tilde{\mathcal{N}}_j)^2 / p_i \tilde{\mathcal{N}}_j$. The test statistic Q approximately follows a χ^2 distribution with $(N_{\mathrm{ADS}} - 1)(N_\xi - 1)$ degrees of freedom.

Across experiments, we found that the ADS distribution is statistically independent from the ADS distribution; see Table I. This proves that ADS acts independently of stochastic noise to produce phenotypic diversity in populations. It also shows that the diversity in doubling times introduced by ADS shapes the population-distribution of doubling times by providing a deterministic "backbone" distribution which is widened further by random noise. Because the population benefits from more diversity, this suggests synergistic benefits to the population could emerge from the combination ADS and noise.

B. Analytical model for deterministic ADS population dynamics

The statistical independence of ADS and stochastic effects allows us to analytically investigate the impacts of ADS in isolation before addressing the effects of the interaction with stochastic diversity. To this end, we developed an analytical model to analyze the deterministic ADS. Most previous analytical treatments of growing populations focus on effects of stochastic dynamics either along lineages or the environment [34–39] and converge on entropy of lineages for increasing population growth. Work on ADS has been focused on the low-asymmetry regime and included effects such as cell-size control [29,40,41] or on individual lineages isolation [13]. In our model, we sought to describe how single-cell ADS inheritance dynamics shape the growth of the population and variations in single-cell doubling time and damage.

We considered the simplest possible model for ADS which describes a clonal population growing in an environment with

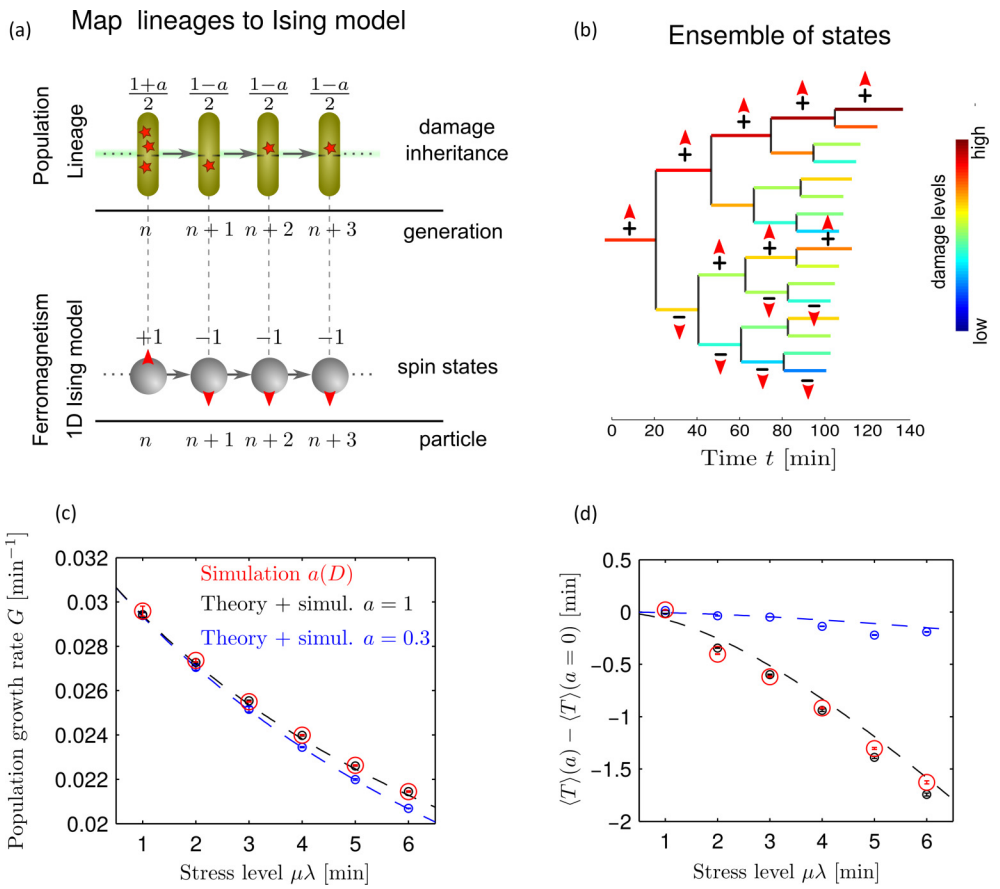

FIG. 2. Mapping of population with asymmetric damage segregation to statistical physics. (a) Schematic illustration of the analogy between lineages in a growing population and 1D Ising model [illustrated lineage is the same highlighted by green shade in Fig. 1(a)]. For a lineage, the history of damage inheritance corresponds to a unique configuration of spins on an Ising chain. The damage accumulation/evasion events shown above each cell [their fraction of inheritance of ancestor damage via Eq. (3)] correspond to the values of the spins (± 1, red arrows) in the analogous Ising chain. (b) Each lineage in a population tree maps to a microstate in an Ising model. Select lineages are marked with the corresponding spin states as in panel (a). (c) Population growth rate as predicted by the theory [lines, Eq. (6)] agrees with numerical simulations (circles), as illustrated for $a = 0.3$ (blue, bottom line) and $a = 1$ (black, top line). Results for the reported damage-dependent asymmetry, $a(D)$ ([16], red, large circles) overlap with those for $a = 1$. Both $t_{\min} = 22$ min and $\mu\lambda$ are in relevant ranges for *E. coli* under experimental conditions [16]. (d) The population growth gain from ADS increases with stress for low ADS ($a = 0.3$, top dashed line) and high ADS ($a = 1$, bottom dashed line). The growth gain is quantified by the difference of mean population doubling times $\langle T\rangle$ with and without ADS.

constant (sublethal) stress [Fig. 1(a)] [16]. In each generation n, each cell accumulates an amount of damage λ in response to the environmental stress, and in addition inherits $D_{\text{inh}}(n)$ amount of damage from its mother that together add up to the total damage $D(n)$. The doubling time of the cell $T(n)$ is slowed down by the accumulated damage, resulting in the following single-cell model:

$$\begin{aligned} D(n) &= \lambda + D_{\text{inh}}(n), \\ T(n) &= t_{\min} + \mu D(n), \end{aligned} \tag{2}$$

where $t_{\min}$ (a constant) is the shortest-possible cell doubling time set by basal, non-ADS processes and μ is the proportionality constant between damage and doubling time. The single-cell times $T(n)$ are related to the growth rate of the cell γ by $\gamma = \ln 2/T(n)$. Experimental studies of bacteria and yeast suggest that a linear relationship between $T(n)$ and $D(n)$ is a reasonable first-order approximation [11,15,16,42,43]. At division, the amount of inherited damage is determined by

$$D_{\text{inh}}(n+1) = \frac{1 + s_n a}{2} D(n), \tag{3}$$

where $s_n = 1(-1)$ indicates whether a cell in generation n accumulates (evades) damage relative to its sibling [Fig. 2(a), top panel]. The amount of asymmetry is described by the parameter a ($0 \leqslant a \leqslant 1$).

TABLE II. Equivalence table relating Ising model to growing populations with ADS.

Interacting spin particles	Growing pop. with ADS
Microstate	Lineage
Ensemble	Population
Spin up/down ($s_n = \pm 1$)	Inherit larger/smaller fraction of damage $\frac{1+s_n a}{2}$
Single-particle energy	Single-cell doubling time T
Total energy E	Elapsed time t
Number of particles n	Number of generations n
Hamiltonian $\mathcal{H}$	Total lineage time $T_{\rm tot}(n,\{s\}) = \sum_{i=1}^{n} T_i$
Number of states Ω	Number of dividing lineages Ω_L

Despite the simplicity of this single-cell model, deriving expressions for the emergent population dynamics is not straightforward because of the nontrivial coupling between cell-generations and time: Cells from different generations may be present at the same time, e.g., cells dividing at time t_{k+3} in Fig. 1(a) are in generations $n+2$ and $n+3$. We overcame this challenge by drawing on an unexpected connection between the nonequilibrium process of growing populations with ADS and equilibrium statistical physics of ferromagnetic particles (Ising model). In brief, the increment in population size $dN_{\rm cells}(t) = N_{\rm cells}(t) - N_{\rm cells}(t-dt)$ at time t is given by the number of lineages dividing exactly at time t. Thus, the population growth rate can be obtained as the rate of growth of the total number of lineages $\Omega_L(t)$ dividing at time t, which are the lineages where the total accumulated lineage time $T_{\rm tot}(n,\{s\}) = \sum_{i=1}^{n} T(i,\{s\})$ is equal to the elapsed time t, i.e., lineages satisfying $T_{\rm tot}(n,\{s\}) = \sum_{i=1}^{n} T(i,\{s\}) = t$. Using Eqs. (2) and (3) we find (see Appendix B1 for details)

$$T_{\rm tot}(n,\{s\}) \approx n t_{\rm min} + \mu\left(2\lambda n + a\lambda \sum_{i=1}^{n}\left(s_i + \frac{s_{i-1}}{2}\right) + \frac{a^2\lambda}{2}\sum_{i=1}^{n-1} s_i s_{i-1}\right). \tag{4}$$

Mathematically, determining the number of dividing lineages $\Omega_L(t)$ is equivalent to the well-described problem of determining the number of states Ω with a given energy for a 1D system of ferromagnetic particles (Ising model) in equilibrium statistical physics [Fig. 2(a)], i.e., the number of possible ways the Hamiltonian $\mathcal{H}$ of the system evaluates to the energy level E, $\mathcal{H} = E$ [Fig. 2(b) and Table II]. We invoke this by defining $\mathcal{H} = \varepsilon T_{\rm tot}(n,\{s\})$ (ε is a conversion factor between energy and time) and focusing on the large-generation limit of $n \to \infty$ (the thermodynamic limit) where the microcanonical and grand canonical ensembles are equivalent, resulting in the partition function

$$Z \approx 2^n e^{-\beta\varepsilon n[(2-a^2\lambda\mu\frac{9+2a^2}{8}\beta\varepsilon)\mu\lambda + t_{\rm min}]}. \tag{5}$$

We thus are able to derive approximate expressions for an equivalent equilibrium physical system with the same characteristics as the nonequilibrium biological system in the high-temperature limit ($\beta\varepsilon \ll 1$) where ADS has a large influence. In effect, this maps each lineage to a particular microstate in the Ising model [Fig. 2(b)], and a full summary of the equivalence between statistical physics and growing populations with ADS is provided in Table II.

To characterize the emergent population dynamics from deterministic ADS, we derived expressions for the population growth rate $G_{\rm ADS}$, the mean single-cell doubling time $\langle T\rangle_{\rm ADS}$ and the standard deviation of doubling times $\sigma_{T,\rm ADS}$ [Eq. (6)]. The growth rate is derived from the total number of states dividing at time t (see Table II) which is found from the contribution across different generations n as $\sum_n \Omega_L(n,t)$. Since the distributions of Ω_L is narrowly peaked around a generation n^* so we use the saddle-point approximation $\sum_n \Omega_L(n,t) \approx \Omega_L(n^*,t)$ and derive the population growth rate as $G = \frac{1}{t}\ln\Omega(n^*,t)$. Furthermore, we have calculated the mean single-cell doubling time $\langle T\rangle_{\rm ADS}$ and the standard deviation of doubling times $\sigma_{T,\rm ADS}$ using statistical moments of the thermodynamic distribution, i.e., $\langle T\rangle_{\rm ADS} = \sum_{\{s\}} T(n)\, e^{-\beta\mathcal{H}(n,\{s\})}/Z$. Table III lists all approximations used in the derivation of this model and Supplemental Material [44] Fig. S1 shows that the impact of the approximations is small. It is important to note that we aimed to characterize the properties of the "active" part of the population. Thus only dividing cells are included when calculating population averages (see Appendix A1 for detailed argumentation). In other words, the properties of the growing cells, those that are between the division cycles, do not contribute to the averages.

$$\begin{aligned}
G_{\rm ADS}(a,\lambda,\mu,t_{\rm min}) = \tilde{S}(a,\lambda,\mu,t_{\rm min}) &\approx \frac{8\lambda\mu + 4t_{\rm min} - 2\varphi(a,\lambda,\mu,t_{\rm min})}{a^2(9+2a^2)\lambda^2\mu^2},\\
\langle T\rangle_{\rm ADS}(a,\lambda,\mu,t_{\rm min}) &\approx t_{\rm min} + \mu\lambda\left[2 - \tilde{S}\frac{a^2\lambda\mu}{4}(a^2+9) + \tilde{S}^2 a^4\lambda^2\mu^2\frac{27}{8}\right],\\
\sigma_{T,\rm ADS}(a,\lambda,\mu,t_{\rm min}) &\approx \frac{\lambda\mu a}{4}\sqrt{20 + a^2(4 + \tilde{S}\lambda\mu[-44 - 45\tilde{S}\lambda\mu + a^2\{2 + 9\tilde{S}\lambda\mu\}])},\\
\varphi(a,\lambda,\mu,t_{\rm min}) &= \sqrt{2}\sqrt{8\lambda\mu t_{\rm min} + 2t_{\rm min}^2 - \lambda^2\mu^2[9a^2\ln 2 - 8 + a^4\ln 4]},
\end{aligned} \tag{6}$$

TABLE III. Assumptions and simplifications made during derivation of results.

Assumption	Implication
Nearest-ancestor interaction (nearest-neighbor in equivalent physical system) dominates	$D_{\text{tot}}(n,\{s\}) \to 2\lambda n + a\lambda \sum_{i=1}^{n}(s_i + \frac{s_{i-1}}{2}) + \frac{a^2\lambda}{2}\sum_{i=1}^{n-1} s_i s_{i-1}$
High temperature	$\beta\epsilon \ll 1$
Thermodynamics limit	$n \to \infty$
Periodic boundary conditions on Ising chains in equivalent physical system	$s_n = s_1$
Constant environmental stress	λ is a constant
Use saddle-point approximation to solve $\sum_n \Omega(n,t)$	$\sum_n \Omega(n,t) \approx \Omega(n^*,t)$.[a] This picks the single largest-contribution generation as function of a, μ, λ and t_{min}

[a] n^* is the largest summand to $\sum_n \Omega(n,t)$.

where $\tilde{S} = S/(k_B t)$ is the normalized entropy of dividing lineages expressed in terms of the thermodynamic entropy S and the elapsed time t which is a measure of lineage diversity. Furthermore, to obtain a simpler expression for $\sigma_{T,\text{ADS}}$ we assumed in the expression above $t_{\text{min}} \gtrsim 15$ min. An approximate expression valid for all values of t_{min} is given in Eq. (B6). We furthermore use the short-hand notation $\tilde{S}$ instead of $\tilde{S}(a,\lambda,\mu,t_{\text{min}})$ on the right hand-side.

Interestingly, all these population characteristics can be expressed in terms of the entropy of dividing lineages $\tilde{S}$ (population diversity), with the population growth rate G_{ADS} itself being mathematically identical to $\tilde{S}$. Thus, the entropic gain in the population growth rate by ADS alone (the increase in population growth rate driven by lineage entropy) $\Delta G_{\text{ADS}} = G_{\text{ADS}}(a) - G_{\text{ADS}}(a=0)$ is equal to the increase in lineage entropy from ADS $\Delta G_{\text{ADS}} = \tilde{S}(a) - \tilde{S}(a=0)$ (where $\tilde{S}(a=0)$ is given by $\tilde{S}(a=0) = \ln 2/(t_{\text{min}} + 2\mu\lambda)$, see Appendix B3). This deep connection between population diversity and population growth establishes that population growth is driven by entropy of lineages. This effect is similar in concept to the effects from stochastic variations presented by Wakamoto *et al.* [1,36].

We confirmed our theoretical predictions by comparing to an agent-based numerical simulation we introduced in our previous work [16] [Figs. 2(c), 2(d), and 3(a)]. See Appendix C for the details of the simulations. Simulations are in good numerical agreement with the analytical results, also for the reported case of damage-dependent asymmetry $a = a(D) \approx \frac{D^6}{D^6+\text{constant}}$ [16]. The results in Eq. (6), which have been derived for the regime where ADS dominates, exhibit different scaling behavior than results derived around $a = 0$ for models including cell-size control [40,41]. Having verified through simulation that our population-level results also hold when cell-size control mechanisms are included (Appendix D), we have not investigated the differences in scaling further.

Our theoretical results [Eq. (6), Figs. 2(c) and 2(d)] confirm previous findings that while the growth is reduced under higher stresses, asymmetric damage segregation ($a > 0$) ensures faster growth than symmetric ($a = 0$) [13]. Furthermore, the positive impact of ADS *grows* with stress $\lambda\mu$ [Fig. 2(d)], resulting in a dynamic, emergent population-benefit [16] endowing the population with an antifragile stress behavior [45]. This antifragility comes as a result of increased diversification under stress; cells can diversify more when they have more damage to redistribute. Here our analytical results predict that this diversity, measured as the width of the distribution of doubling times, increases linearly with stress $\sigma_{T,\text{ADS}} \sim \lambda$ when $a = 1$ [Fig. 3(a)] and approximately linear for damage-dependent asymmetry $a(D)$, Supplemental Material [44] Fig. S2.

C. Experimental verification of ADS population dynamics

We verified this emergent behavior by analyzing published data for tens of thousand of cells from Stewart *et al.* [10] and ourselves [16] for the stress-dependence of $\sigma_{T,\text{ADS}}$ across three different stresses and three different strains (see Table I). We did this by assessing if the predicted width of the distribution of doubling times $\sigma_{T,\text{ADS}}$ [Eq. (6)]—a key theoretical prediction—was confirmed by the experimental data when correcting for non-ADS stochastic effects. Using the ADS-filtered data, we fitted the deterministic ADS model to each experimental condition and obtained the experienced stress $\lambda\mu$ (see Appendix A2 for methods details). Plotting the experimental values of $\sigma_{T,\text{ADS}}$ against these experienced stresses, we found that the data across conditions was well-described by our theoretical predictions [Fig. 3(b)]. The significantly lower levels of perceived stress in data by Stewart *et al.* [10], compared to our wild type strain [16], both grown at 37 °C, may reflect differences between growing cells in rich (Luria broth [10]) versus minimal media (M63 [16]). In calculating the experimental values of $\sigma_{T,\text{ADS}}$ we used all recorded cells in the growing population since this ensemble gives the same moments but higher cell count than using dividing cells at the last time point (see Appendix A1). This experimental validation of stress-induced deterministic diversification [Fig. 3(b)] together with the damage-structured population [Sec. II A, Figs. 1(c)–1(e)] indicate the strong impact of the deterministic ADS on the population distribution and suggest that the improved conditions for growth it provides are exploited by real populations.

D. Synergistic contributions of stochastic and deterministic diversities to population growth

Having established and validated the population-level model for ADS, we next focused on the central question of

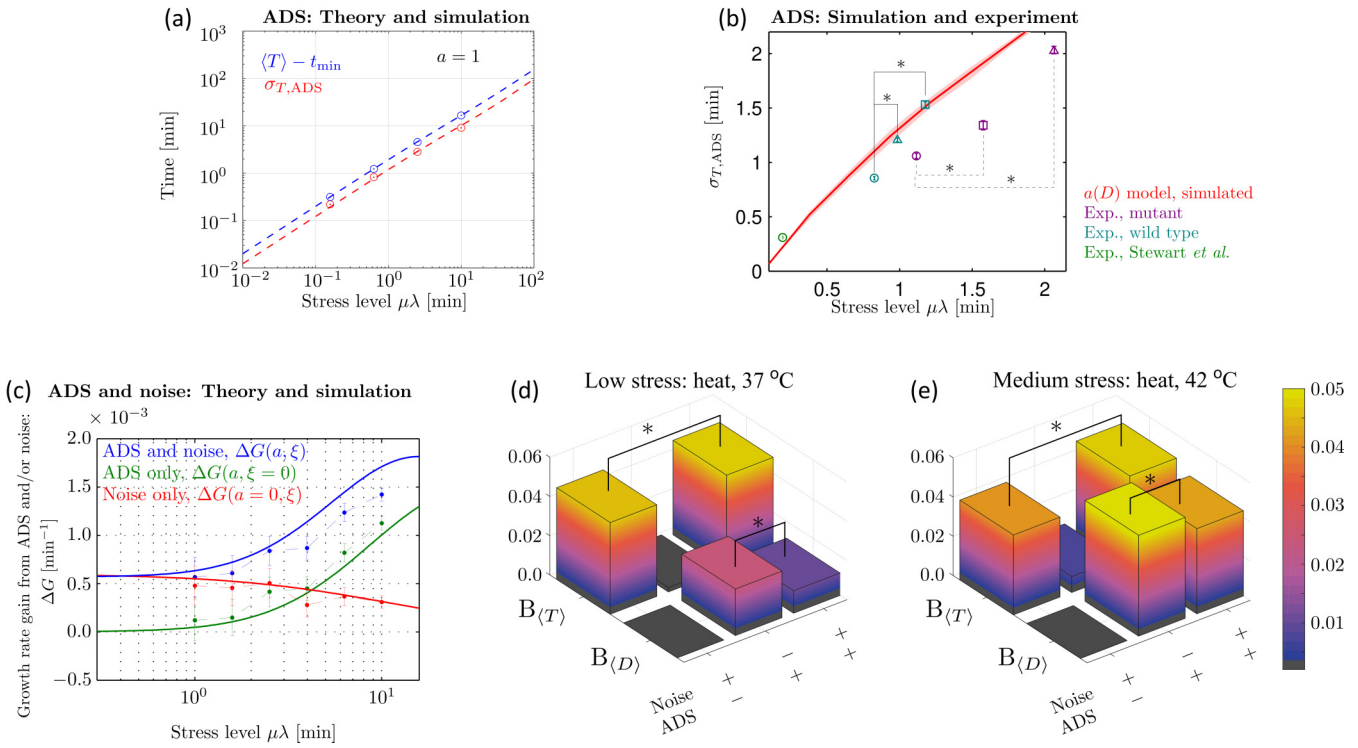

FIG. 3. The interplay of stochastic and deterministic sources of diversity under stress. (a) Analytical predictions [Eq. (6), dashed lines] of a linear increase of the effects of ADS with stress confirmed by simulations (circles), as illustrated by $\langle T\rangle_{\mathrm{ADS}} - t_{\min}$ (top dashed line) and $\sigma_{T,\mathrm{ADS}}$ (bottom line). Errorbars show sample error of the means from the simulations (Appendix C). The same trends hold for damage-dependent asymmetry, although exact linearity is not satisfied, see Supplemental Material [44] Fig. S2. (b) Comparison of model predictions for $\sigma_{T,\mathrm{ADS}}$ with experimental results across all stresses. Squares mark heat-stress, triangles antibiotic (kanamycin) stress and circle marks low UV stress (Stewart *et al.* [10]). Perceived experimental stress levels $\mu\lambda$ are inferred by fitting the model to the ADS-filtered data (Methods). Each mark represents the average over all cells with those particular experimental conditions, while the red line is the simulation results from 100 repeat simulations of $a(D)$-model (line indicates 50th percentile, with the shaded region indicating 25th−75th percentile). **C** Synergistic contributions of noise and ADS to the population growth rate. Points mark simulation results, while lines are the analytical results [Eq. (7)]. The gain in population growth from noise alone, $\Delta G(a=0,\xi)$, is in green [Eq. (E8); bottom line at small $\mu\lambda$]; from ADS alone, $\Delta G(a=1,\xi=0)$, is in red [Eq. (6); decreasing middle line] and from combined noise and ADS, $\Delta G(a=1,\xi)$, is in blue [Eq. (7); top line]. Errorbars mark 95% confidence interval on fitting exponential growth to the number of cells across 10 repeat simulations (Appendix C2). (d), (e) Benefits of doubling time, $B_{\langle T\rangle}$, and damage, $B_{\langle D\rangle}$, defined in Eq. (8), under various combinations of noise and ADS in a case of low (d) and medium (e) damage induced by heat stress [16]. While the population benefits from both noise and ADS in reducing population doubling time (compare results for $B_{\langle T\rangle}$), noise antagonizes the beneficial effects of ADS in decreasing population damage (compare results for $B_{\langle D\rangle}$). For simulations with noise, we show the mean across 10 realizations. Here the asymmetry is set to be damage-dependent, $a(D)$; however, results are similar for $a = 1$. Asterisks indicate statistically significant differences with $p < 5.0\times10^{-8}$ (bootstrap, t-test, see Appendix A3).

the interaction between the deterministic diversity from ADS and random, stochastic noise. To investigate this we analyzed the entropic gain for the population growth rate, i.e., the changes in population growth rate to modulations in lineage diversity $\tilde{S}$. In other words, we consider the increase in population growth rate $\Delta\tilde{G} = G(a,\xi) - G(a=0,\xi=0)$, where ξ denotes noise, and where lineage entropy is controlled via noise level ξ and asymmetry a. Adding noise to the model in Sec. B is not straightforward, so to answer this question we turned to the Euler–Lotka model of population growth which allowed us to relate the *population diversity* resulting from the combined existence of ADS and noise [with the probability density of doubling times $f_{\mathrm{full}}(T_{\mathrm{ADS}}, T_\xi)$] to *population growth* $G(a,\xi)$ [46–48]. Since the distributions of noise and ADS-induced doubling times are statistically independent (Sec. II A) we found a simplified expression for $G(a,\xi)$ by expanding each of these distributions in statistical cumulants and applying series inversion [49,50] (Appendix E1). To account for the fact that noise amplitudes scale with stress (we assume coefficient of stochastic variations, C_V in single-cell growth rates to be conserved across stresses), we scaled the noise amplitude relative to the mean doubling time $\langle T\rangle_{\mathrm{ADS}}$ (Appendix E), resulting in the final expression

$$\begin{aligned}\Delta\tilde{G} &= G(a,\xi) - G(a=0,\xi=0)\\ &\approx \frac{\ln 2}{\langle T\rangle_{\mathrm{ADS}}} + \frac{1}{2}\left[\frac{\sigma^2_{T,\mathrm{ADS}}}{\langle T\rangle_{\mathrm{ADS}}} + C_V^2\langle T\rangle_{\mathrm{ADS}}\right]\left(\frac{\ln 2}{\langle T\rangle_{\mathrm{ADS}}}\right)^2\\ &\quad - \frac{\ln 2}{t_{\min} + 2\mu\lambda},\end{aligned} \tag{7}$$

where $\langle T\rangle_{\mathrm{ADS}}, \sigma^2_{T,\mathrm{ADS}}$ are given by Eq. (6), $G(a=0,\xi=0) = \frac{\ln 2}{t_{\min}+2\mu\lambda}$ (Appendix B3) and $C_V = 0.23$ is inferred from experimental data in Ref. [16] (available in Supplemental

Material [44] Sec. III.10). These analytical results [Eq. (7), Fig. 3(c), blue line] capture the general trend of the simulated results [Fig. 3(c), blue (top) and red (decreasing) dots].

With all parameters constrained by the data, our analytical and simulation results show that the relative importance of the deterministic ADS and stochastic processes in shaping the population growth changes with stress [green (bottom) and red (decreasing) lines in Fig. 3(c)]. At low stresses, the benefit from ADS (green; bottom) is small and noise (red; decreasing) dominates, while ADS dominates for large stresses. Even when noise dominates, ADS remains present and contributes as illustrated by our results in Sec. II A. The experimental estimates of the perceived stress $\mu\lambda$ [Fig. 3(b)] all fall below the cross-over point, $\mu\lambda_c \approx 4$, suggesting that noise dominates in the tested conditions. Furthermore, the estimates of the perceived stress allow us to read off the relative contributions of deterministic and stochastic components [Fig. 3(c)] for each of the experimental conditions. Thus, for example, in mutant cells experiencing kanamycin stress with $\mu\lambda \sim 2$ [triangles in Fig. 3(b)], ADS accounts for about 24% of the gain in growth rate, $\Delta\tilde{S}$. While the contribution from ADS is minor, it is significant [Figs. 3(c)–3(e)] and may dominate under the experimental conditions where perceived stresses are higher.

E. Stochastic and deterministic effects *antagonize* each other in reducing population damage levels

We have previously shown that by concentrating damage in a few slowly growing cells, ADS decreases the average damage in a population [16]. We then asked how the measured levels of noise impact the ADS-induced reduction in population damage and mean doubling time.

To quantify the effects we considered how the population benefits from the diversity generated by either noise alone, ADS alone, or both ADS and noise combined. We use the case with $a = 0$ and "no noise" ($\xi = 0$) as a reference point and define benefits as the decrease in population damage and mean doubling times relative to their reference values:

$$B_{\langle T\rangle} = 1 - \frac{\langle T\rangle(a,\xi)}{\langle T\rangle(a=0,\xi=0)},$$
$$B_{\langle D\rangle} = 1 - \frac{\langle D\rangle(a,\xi)}{\langle D\rangle(a=0,\xi=0)}, \quad (8)$$

here $B_{\langle T\rangle}$ and $B_{\langle D\rangle}$ are the benefits from the diversity in the population-mean doubling time $\langle T\rangle$ and damage $\langle D\rangle$.

Please note that the benefit scores defined here are different from the ones in Ref. [16], as the current formulation is more intuitive showing an increase in benefit with increasing stress.

The results [Figs. 3(d) and 3(e)] for *E. coli* doubling times mirrored our results for the entropic gain in population growth rate [Fig. 3(c)]. The benefit in doubling time is dominated by noise $B_{\langle T\rangle} \sim 0.04$ and ADS provides a minor but statistically significant increase of ∼0.01. The roles of ADS and noise are, however, distinctly different in reducing population damage. While ADS alone significantly reduces population damage, with $B_{\langle D\rangle} \sim 0.05$ at higher stress, noise antagonizes this effect decreasing the benefit by ∼0.01 [Figs. 3(d) and 3(e)].

To understand these seemingly contradictory outcomes of noise, consider the dynamics along a single lineage. Without noise, cells which consecutively inherit the new-pole [$s_n = -1$ in Eq. (3)] will have less damage and will divide faster. However, in the presence of noise, this is no longer the case: Noise interferes with the ordered chains of damage inheritance through the lineages so that it is no longer cells with the lowest amounts of damage that have the shortest doubling times; even though the average noise contribution along each lineage is zero, the fastest-dividing cells—those which drive the population growth—will on average have more damage when noise is present. Consequently, the average damage $\langle D\rangle$ is higher when noise is present, leading to lower benefits $B_{\langle D\rangle}$.

III. DISCUSSION

While our study has been focused on *E. coli*, the deterministic and stochastic processes driving the discovered dynamics are more widely present across unicellular and multicellular organisms. Stochastic noise is ubiquitous in cell populations [5,51] and more recent findings have established that ADS—asymmetric partitioning of damaged proteins resulting in slower growth of cells inheriting damage—also appear to be a general phenomenon [9,11,12,18–25]. A particularly striking example is the mammalian neuronal stem cells [25], where much like in rejuvenated bacterial cell, by segregating damage to the nondividing neuron, the stem cell reduces damage and avoids senescence.

We have found the following key results. First, we analytically show that stress induces deterministic cell-cell variability through ADS which, in turn, results in deterministic changes to population growth [depends explicitly on the entropy of lineages $\tilde{S}$, Eq. (6)]. Compared to most other studies, this variability is deterministic and correlated through generations, yet the effects on population growth are similar to those endowed by noise alone [1,36]. The impact of slow-growing cells harboring more damage reduces as the population grows, i.e., they have smaller overall impact. Being an emergent property from just the inheritance dynamics, we expect that the population benefits can be found across all cell types with ADS. For neuronal stem cells where damage is segregated to the nondividing neuron, the upshot of ADS is that the dividing cells grow faster enabling more rejuvenation for the organism.

Second, our analyses show that while operating on different time-scales, both the deterministic (ADS) and stochastic (noise) sources of diversity accelerate population growth (as compared to a nondiversified population) and their effects add up. It furthermore suggests that the "speed limit" on population growth proposed by Hashimoto *et al.* [1] can be circumvented if multiple sources of diversity are present.

Under varying stresses, the additive effect provides the population with the best of both contributions: under low stress the growth-benefit from diversity is dominated by the noise, while the benefits of ADS become more prevalent under higher stresses yet retaining the baseline growth benefit from noise. We find that in all the investigated experimental conditions the stress is not high enough for the deterministic component to dominate, however, even under the lowest perceived stress (low-level UV stress by Stewart *et al.*), the contribution of ADS is nonetheless significant [Figs. 1(c) and 1(d)]. Recently, Proenca *et al.* [8] estimated that in a stress-free environment deterministic sources contribute 22% to the variance of the doubling times. Although the numbers are not

directly comparable to ours due to differences in experimental systems, our results agree on that noise dominates distribution of doubling times under lower stresses and as a consequence has a major contribution to the entropic gain in population growth rate.

Third, while the deterministic and stochastic components both accelerate population growth, they have the opposing effects on population damage. Deterministic ADS reduces population damage because it effectively limits damage to a few slowly growing cells. Stochastic variations in cell's growth rates counteract this effect because they disrupt the coupling between cell's doubling times and damage levels (stochastically, cells with damage may grow fast and generate more damage-containing progenitors). This interplay between stochastic and deterministic variations suggest that to minimize both population doubling time and mean damage, there should be an optimal level of stochastic variations. With the general applicability of ADS, it would be exciting to test this hypothesis across cell types.

These findings are limited to populations where all lineages are present, i.e., to sublethal stress levels. Beyond this, cells die and disappear from the population, and thereby stop some of the lineages which drive the ADS benefits. The remaining lineages will continue to deliver some damage alleviation, but the analytical results no longer hold. This may furthermore also affect the interplay between stochastic and deterministic sources of diversity so it is an open question if the combination of synergistic and antagonistic effects will persist (our third key result). It will be interesting to pursue these questions in separate studies.

As our mathematical models for ADS, and ADS and noise combined, are based on simplistic formulations and generally applicable frameworks, we anticipate that these three key results will persist when other independent sources of variability (stochastic and deterministic) are at play (e.g., multivariate noise or other types of cellular damage, not limited to protein aggregates). We furthermore also expect that the models can also be used as a general framework for studying ADS across organisms and cell types.

A. Potential application of findings to drug-tolerance

We finish with a speculative application of our findings to a practical case of significant impact on public health. Single-cell studies on drug tolerance suggest that there is a common theme across drugs and organisms: A small fraction of the population in a dormant state—cells growing slowly or completely arresting their growth—survive exposure to drugs [52,53]. Several mechanisms have been proposed to explain the emergence of the tolerance: from diversity in lag times and growth rates to toxin-antitoxin regulatory networks [53,54]. Similar studies in cancer cells are slowly emerging [52]. While these "executive" mechanisms are different, most are assumed to be a result of bet-hedging—initiated by stochastic fluctuations in protein numbers [3]. Alternate to random bet-hedging, the dormant cells (and thus drug-tolerance) may be generated by the deterministic processes such as asymmetric damage segregation [8,16] or asymmetric partitioning of the multidrug efflux pump (AcrAB-TolC) towards the old pole [55].

Understanding the interplay between the stochastic and deterministic sources of diversity (of which tolerance-associated dormancy is a specific case) can influence the development of the novel antibiotic strategies. If the origin of the diversity is stochastic, then we can estimate how many but *not which* cells become tolerant, whereas if it is *deterministic*, then we can, in principle, predict *both how many and which cells* are likely to become tolerant. Thus, for example, in the cases of asymmetric damage or AcrAB-TolC partitioning the pole-age, the size of protein aggregates may serve as a marker for dormancy and thus tolerance. In line with this, recent findings show that cells with aggregates are more likely to tolerate otherwise lethal stresses [56]. In this context, the uncovered correlation between damage-history score and doubling time suggests that slow growth in several consecutive generations may serve as another marker for old-pole and dormancy. Experimentally, this possible link between damage-history, dormancy and antibiotic tolerance can be assessed by fluorescent pulse-labeling of the cell wall [57].

ACKNOWLEDGMENTS

We thank Eric J. Stewart for kindly sharing his data from Ref. [10], and we also thank Ariel Amir for a critical reading of the manuscript.

APPENDIX A: EXPERIMENTAL DATA ANALYSIS

1. Sampling growing populations: Statistical ensembles to calculate instantaneous population averages

Picking out exactly the dividing cells at a particular point in time is key to correctly sampling the data, especially when it comes to the statistical moments ($\langle T\rangle$, $\sigma_{\langle T\rangle}$, $\langle D\rangle$, $\sigma_{\langle D\rangle}$ and the benefits $B_{\langle T\rangle}$ and $B_{\langle T\rangle}$), which we describe here. *The main takeaways from this analysis is that all historical cells can be used to calculate population moments at a particular point in time.*

We have used our simulations to study which ensembles to use; see Fig. 4. In the results below we focus on the impact on damage, but similar results are found for doubling times; this is as expected given the connection between these two quantities as stipulated by Eq. (2). We first define the interrogation time T_0 which corresponds to the exact time at which the ADS population model is applied (i.e., it corresponds to setting $t = T_0$). Using T_0, we define the following three statistical ensembles

(1) *Ensemble 1*: Compiling all cells dividing at any time in the in time interval $[0; T_0]$.

(2) *Ensemble 2*: All cells dividing in the narrow interval ΔT around T_0, $[T_0 - \frac{\Delta T}{2}; T_0 + \frac{\Delta T}{2}]$.

(3) *Ensemble 3*: All cells dividing after T_0, $]T_0; \infty[$.

Ensemble 2 is the naïve approximation to the instantaneous ensembles used in the theory. Using this ensemble to calculate statistical moments gives the correct mean behavior as can be seen from the green lines in Figs. 4(b) and 4(c). However, although population moments calculated from Ensemble 2 gives the right average behavior, the uncertainty is higher because this ensemble contains a smaller number of cells.

Surprisingly, Ensemble 1 gives the same mean behavior for all relevant statistical moments as Ensemble 2; to see

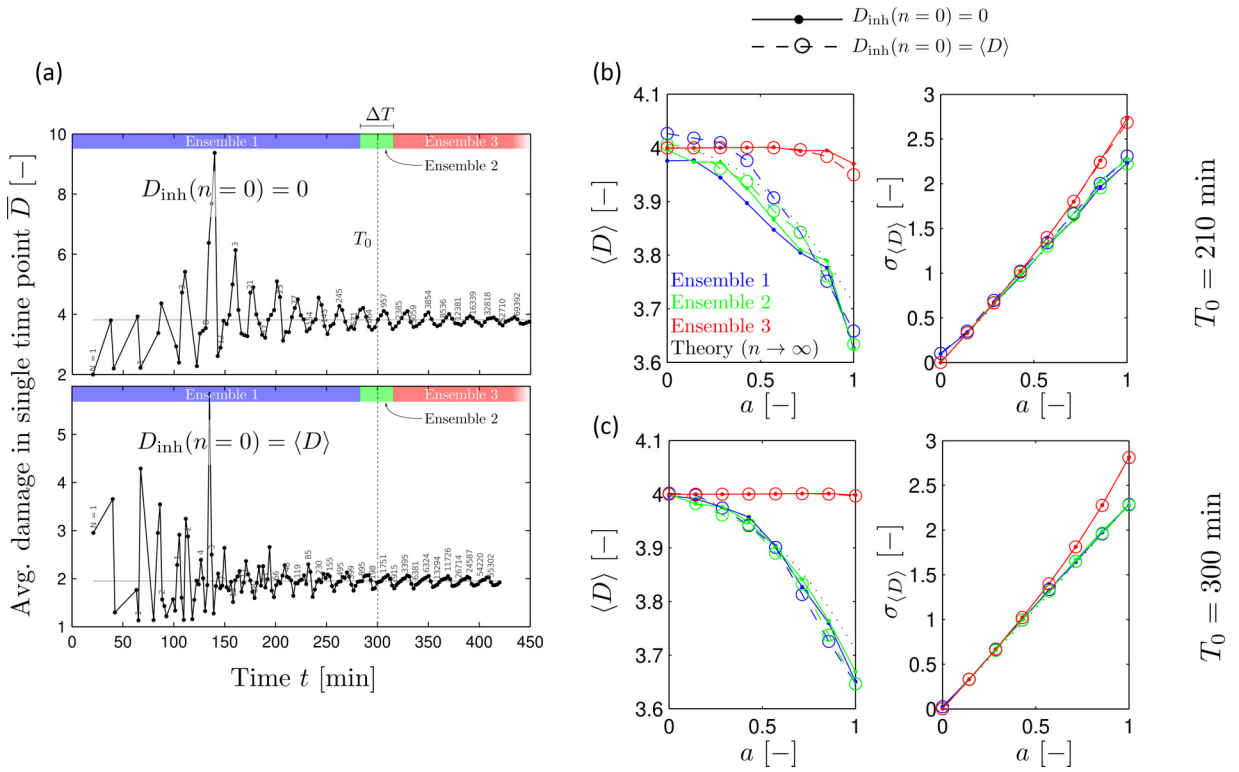

FIG. 4. Illustration of the three ensembles from Appendix A 1 for sampling data from experiments or simulations, with the data in the figure coming from simulations using $(\lambda, \mu, t_{\text{min}}) = (2, 1, 18\ \text{min})$ corresponding to the parameters of the experimental conditions under highest stress (mutant MC4100ΔclpB strain exposed to antibiotic stress [0.05 μG/ml kanamycin)]. Using either ensembles 1 (blue) or 2 (green) to calculate the moments replicates the results of our theory (dotted lines) presented in Eq. (6), but ensemble 3 (red) gives the results without ADS. (a) Time evolution of the instantaneous values $\overline{D}$ of the mean-population damage computed based on all cells dividing exactly at the sampling time t using $a = 0.8$, with the number of dividing cells indicated for every fifth data point. $\overline{D}$ (black) converges towards the theoretical population mean $\langle D\rangle$ from Eq. (6) (gray line) and settles after about 150–200 min, although some fluctuations persist beyond this, for both the case where the initial cell in the population has 0 damage (top panel) and when the population starts from a cell with the average damage (bottom panel). (b), (c) Results for the population mean damage $\langle D\rangle$ and standard deviation of damage $\sigma_{\langle D\rangle}$ for each of the three ensembles (colors) and compared to theoretical results (black dotted lines). At both investigation times $T_0 = 210$ min (b) and 300 min (c) we find good agreement between theoretical predictions from Eq. (6) for infinite population (black dotted line) and the results from the finite simulations using either ensembles 1 (blue) or 2 (green) for both initial conditions for the simulations (compare dashed and full colored lines).

this, compare blue lines to green lines (dashed or full). This observation can be explained by a combination of two different facts. First, the instantaneous averages $\overline{D}$—the averages calculated at just a single point in time—converge to the long-term population average rather quickly, see Fig. 4(a), which suggests that the underlying distributions are similar. Therefore, adding together the underlying distributions at all these times before calculating the moments simply increases the population on which to calculate the moments. Second, because of the exponential growth in the number of dividing cells with time, the vast majority of the cells is from the few last time points sampled; thus, any influence in skewing the moments from the accumulated distribution from Ensemble 1 becomes increasingly small at longer simulation times.

Ensemble 3, however, gives very different results as can be seen from the red lines in the figure: instead of converging to the theoretical results, moments computed from this ensemble do not contain any of the benefits of ADS; in fact, they very explicitly give the results of no ADS ($a = 0$) presented in Appendix B 3. The reason for this is that Ensemble 3 includes all cells from all generations, whereas the beneficial contributions from ADS are driven by the "upconcentration" of cells of shorter lifetimes across different generations via positive feedback in single-cell growth; by sampling all cells across all times, the upconcentration driven by ADS is removed.

Based on these findings we have used Ensemble 1 for all experimental results in this paper since it gives truthful results for population moments while also reducing the uncertainty.

2. Inferring experimental stress levels and noise distribution ξ

Perceived stress $\mu\lambda$ of experiments were inferred by fitting out discrete, agent-based ADS simulation model to noise-filtered experimental doubling times (filtered using Eq. (1) with the damage-dependent asymmetry $a(D)$; see Ref. [16]). Starting from a single cell, the simulation model was fitted using least-squares at all generations along all lineages using the noise-free simulations instead of the theoretical results from Eq. (6) to better utilize all the information. For data from Ref. [10] we fixed t_{min} (cannot be inferred independently) and fitted μ and λ; for data from Ref. [16] we fixed μ for pairs of

experiments with same stressor but different stress levels and allowed λ to take different values at each settings. $t_{\min}$ and a were kept fixed for all experiments.

Using above fitting procedure we obtained population-optimal values for μ and λ allowing us to predict the doubling time for each cell in each population.

3. Statistical significance of increase in σ under different stresses

Calculating the statistical significance of the difference of widths σ of population-distributions of ADS doubling times T^{ADS} under different stresses [Fig. 3(b)] is complicated by the fact that the ADS null distributions also change between experiments. These null distributions are obtained by randomly shuffling cells between lineage bins and then applying the ADS filtering afterwards [Eq. (1)]; see details of null distributions in Ref. [16].

To account for the varying null distributions we calculated the statistical significance of increases in width using bootstrapping. Thus, we computed the statistical significance of the difference

$$\Delta\sigma = \sigma^{\text{high stress}} - \sigma^{\text{low stress}}, \tag{A1}$$

for both bacterial strains (ΔClpB mutant and WT) and both types of stress (heat and kanamycin).

APPENDIX B: MATHEMATICAL POPULATION MODEL FOR ASYMMETRIC DAMAGE SEGREGATION

1. Expressions for damage and doubling time for individual cells and the whole lineage

For motivation, we first write out the damage in the first few generations for a population starting with a single cell with 0 initial damage,

$$\begin{aligned}
&\text{Generation 1}: \quad \lambda,\\
&\text{Generation 2}: \quad \lambda\left[\frac{1+s_2a}{2}+1\right],\\
&\text{Generation 3}: \quad \lambda\left[\left(\frac{1+s_3a}{2}\right)\left[\frac{1+s_2a}{2}+1\right]+1\right],
\end{aligned}$$

where s_i denotes the sign multiplying the asymmetry parameter a as in Eq. (3) ($s_i = \pm 1$). This sign s_i indicates the spin state. This leads to the following expression for the damage in generation n of any cell starting form a single cell with 0 damage in generation

$$\begin{aligned}
D(n,\{s\}) &= \lambda\Big[1+\frac{1+s_na}{2}+\left(\frac{1+s_na}{2}\right)\left(\frac{1+s_{n-1}a}{2}\right)\\
&\quad+\left(\frac{1+s_na}{2}\right)\left(\frac{1+s_{n-1}a}{2}\right)\left(\frac{1+s_{n-2}a}{2}\right)+\ldots\Big],
\end{aligned} \tag{B1}$$

$$= \lambda\left[1+\sum_{j=1}^{n}2^{-j}\left(\prod_{k=n-j+1}^{n}\{1+s_ka\}\right)\right], \tag{B2}$$

where the dependence on $\{s\}$ indicates that each possible combination of the signs s_i provides a new solution. From Eq. (2) we find for the associated single-cell doubling time to the damage given in Eq. (B2),

$$T(n,\{s\}) = t_{\min} + \mu\lambda\left[1+\sum_{j=1}^{n}2^{-j}\left(\prod_{k=n-j+1}^{n}\{1+s_ka\}\right)\right]. \tag{B3}$$

Clearly, the damage and doubling time of each cell depends on its entire lineage history because of the inheritance.

To derive results for the whole lineage, we first focus on the total lineage damage $D_{\mathrm{tot}}(n,\{s\})$ as a function of generation number n from Eq. (B2),

$$\begin{aligned}
D_{\mathrm{tot}}(n,\{s\}) &= \sum_{q=1}^{n} D(q)\\
&= \sum_{q=1}^{n}\lambda\left[1+\sum_{j=1}^{q}2^{-j}\left(\prod_{k=q-j+1}^{q}\{1+s_ka\}\right)\right].
\end{aligned} \tag{B4}$$

It is clear that each division adds more complexity to the problem, as it introduces the *possibility* that even more damage levels (and hence cell doubling times) can be reached by the population. However, due to the factor 2^{-j}, the importance of the previous generations decays approximately exponentially; consequently, we may approximate Eq. (B4) by writing out all terms in Eq. (B2) and truncating after terms proportional to s_{n-1} (truncating contributions beyond nearest ancestor (nearest neighbors in the equivalent physical system),

$$D_{\mathrm{tot}}(n,\{s\}) \approx 2\lambda n + a\lambda\sum_{i=1}^{n}\left(s_i+\frac{s_{i-1}}{2}\right)+\frac{a^2\lambda}{2}\sum_{i=1}^{n-1}s_is_{i-1}, \tag{B5}$$

where the geometric series, e.g., $\lambda(1+\frac{1}{2}+\frac{1}{4}+\frac{1}{8}+\ldots)$, have been approximated by their limiting values, $\lim_{n\to\infty}\lambda\sum_{i=0}^{n}2^{-i} = 2\lambda$. Although these approximations may seem very limiting, we show in Sec. S2 in the Supplemental Material [44] that the error is only on the order of a few percent. The expression for $D_{\mathrm{tot}}(n,\{s\})$ above together with Eq. (2) lead to Eq. (4).

2. Supporting expression for $\sigma_{T,\mathrm{ADS}}$ and expressions for population moments of damage

The full expressions for the width $\sigma_{T,\mathrm{ADS}} = \sqrt{\langle T(n)^2\rangle - \langle T(n)\rangle^2}$ applicable for all values of $t_{\min}$ [extending the simplified expression presented in Eq. (6)] is

$$\sigma_{T,\mathrm{ADS}} \approx \frac{\mu\lambda a}{4}\sqrt{20+a^2[4+\beta^*\varepsilon\lambda\mu(-44-45\beta^*\varepsilon\lambda\mu+a^2\{2+9\beta^*\varepsilon\lambda\mu[1+\beta^*\varepsilon\lambda\mu(27+a^2\{2-18\beta^*\varepsilon\lambda\mu\})]\})]}, \tag{B6}$$

where

$$\beta^*\epsilon = \frac{\ln \Omega(t, n^*)}{t} = \frac{8\lambda\mu + 4t_{\min} - 2\,\varphi(a, \lambda, \mu, t_{\min})}{a^2(9 + 2a^2)\lambda^2\mu^2}, \tag{B7}$$

and $\varphi(a, \lambda, \mu, t_{\min})$ is defined in Eq. (6).

Furthermore, results for the moments of damage distribution across the population can be derived analogously, resulting in

$$\begin{aligned}\langle D(n)\rangle &= \frac{\langle T(n)\rangle - t_{\min}}{\mu} \\ &= \lambda\Bigg[2 + \frac{1}{(9 + 2a^2)^2\lambda^2\mu^2}[\varphi(a, \lambda, \mu, t_{\min}) \\ &\quad - 4\lambda\mu - 2t_{\min}][27\varphi(a, \lambda, \mu, t_{\min}) - 54t_{\min} \\ &\quad + (27a^2 - 27 + 2a^4)\lambda\mu]\Bigg]\end{aligned} \tag{B8}$$

$$\sigma_{D,\mathrm{ADS}} = \frac{\sigma_{T,\mathrm{ADS}}}{\mu}, \tag{B9}$$

where $\sigma_{T,\mathrm{ADS}}$ is given by Eq. (B6).

3. Exact analytical treatment of the special case for $a = 0$

The special case of symmetric division ($a = 0$) is not handled by our approximate analytical expressions because the high-temperature approximation becomes invalid for $a = 0$ (all cells are completely identical—carrying the same amount of damage and dividing at the same time—so all lineages are degenerate and our statistical physics approach no longer apply). However, noting that in this special case average population-properties are identical to single-cell properties, we can easily provide exact analytical expressions for the population behavior.

Inheriting exactly 50% of the ancestor's damage ($a = 0$), the damage in generation n of a single cell starting from 0 damage at the first generation is given by

$$D(n) = \lambda \sum_{j=1}^{n} \frac{1}{2^{j-1}} = 2\lambda \quad \text{for} \quad n \to \infty. \tag{B10}$$

In this large-generation limit all cells in the population have the same amount of damage, and so

$$\langle D\rangle = 2\lambda \quad \text{and} \quad \sigma_D = \sqrt{\langle D(n)^2\rangle - \langle D(n)\rangle^2} = 0, \tag{B11}$$

where σ_D is the standard deviation of the population-distribution of damage. From Eq. (2) we find for the distribution of doubling times

$$\langle T\rangle = t_{\min} + \mu\langle D\rangle = t_{\min} + 2\mu\lambda \quad \text{and} \quad \sigma = \mu\sigma_D = 0. \tag{B12}$$

Finally, we derive an expression for the population growth rate and normalized entropy (in the same limit of $n \to \infty, t \gg 1$),

$$\begin{aligned} N_{\mathrm{cells}} &= 2^{\frac{t}{\langle T\rangle}} = e^{Gt}, \\ G &= \frac{\ln 2}{\langle T\rangle} = \frac{\ln 2}{t_{\min} + 2\mu\lambda}, \\ \tilde{S} &= \frac{S}{k_B t} = \frac{\ln \Omega_L}{t} = G = \frac{\ln 2}{t_{\min} + 2\mu\lambda}. \end{aligned} \tag{B13}$$

APPENDIX C: SIMULATION DETAILS

We relied on our previously described brute-force simulation approach [16]. Briefly, this method builds out the full population tree up to N_{gens} generations, and calculates for each cell the amount of damage and the doubling time based on the basic inheritance rules of Eq. (2), using either constant asymmetry a or damage-dependent asymmetry $a(D)$. From this we can assign to each cell k in generation n the birth time $\tau_k^{\mathrm{birth}}(n)$ and death time $\tau_k^{\mathrm{death}}(n)$ [with $\tau_k^{\mathrm{death}}(n) = \tau_k^{\mathrm{birth}}(n) + T_k(n)$ where $T_k(n)$ is the single-cell interdivision time], as well as the damage $D_k(n)$.

To speed up convergence of the simulations for cases without experimental noise ξ, low-amplitude noise [sampled from $\mathcal{N}(0, \frac{1}{5}t_{\min})$ normal distribution] is added to $\tau_k^{\mathrm{birth}}(n)$ for all cells present between generations 2 and 5.

1. Adding experimental non-ADS noise ξ

We obtained experimental noise distributions f_ξ from Eq. (1), and applied this noise in simulations by extending the single-cell growth [Eq. (2)] with additive noise ξ_n sampled from the experimental noise distribution,

$$T(n) = t_{\min} + \mu D(n) + \xi_n. \tag{C1}$$

Our earlier results suggested that the the coefficient of variation $C_V = \sigma_\xi/\langle T\rangle$ for the standard deviation of the noise σ_ξ increased slower that the C_V for the deterministic variations (about twofold difference [16]). For simplicity, we assumed a constant coefficient of variation from stochastic sources and scaled the experimental noise ξ_n at different stress levels with the respective mean. We implemented this in the simulations for a given set of a, $t_{\min}$, μ and λ by scaling the noise f_ξ^λ at any stress λ according to $C_V\,\langle T\rangle$ with the theoretical mean $\langle T\rangle$ from Eq. (6),

$$f_\xi^\lambda = f_\xi^{\lambda(42\,^\circ\mathrm{C})}\frac{C_V\,\langle T\rangle(\lambda)}{\sigma_\xi(42\,^\circ\mathrm{C})}, \tag{C2}$$

where $C_V = 0.23$ and using the data from the mutant cell line at 42 °C as reference.

2. Simulation data analysis: Calculating population properties

a. Growth rate

The number of cells in the population grows exponentially in time $N_{\mathrm{cells}}(t) \propto e^{Gt}$ so we fit a linear model $y(t) = \theta_1 t + \theta_0$ to the logarithm of $N_{\mathrm{cells}}(t)$ using Matlab's `fit` procedure from the Curve Fitting Toolbox to obtain the population growth rate from the simulations while minimizing the influence of the last few time points. We omitted the first part of the simulations to minimize the influence of the first few cells, and we obtained the standard error SE_G on the fitted values of G directly from the built-in `confint` function.

b. Normalized entropy

Since the normalized entropy $\tilde{S} = \frac{S}{k_B t}$ is equal to the population growth rate for both ADS and noise (see Eq. (B7) and Refs. [1,36]), we obtain this from the simulations as described for the population growth rate. For differences of normalized entropies $\Delta\tilde{S} = \frac{S(a\geqslant 0, \alpha\geqslant 0)}{k_B t} - \frac{S(a=0,\alpha=0)}{k_B t}$ we

calculate the standard error via error propagation $\mathrm{SE}_{\Delta\tilde{s}} = \sqrt{\mathrm{SE}^2_{G(a\geqslant 0,\alpha\geqslant 0)} + \mathrm{SE}^2_{G(a=0,\alpha=0)}}$.

For repeat simulations [Fig. 3(c)], average results were obtained as follows. Since linear regression is used to infer the values of G from the simulations, this point estimate has a Gaussian sampling distribution [58] and so the average estimate across N_{rep} independent simulations can be obtained as the average across the underlying sampling distributions from each estimate. Additionally, since this distribution is also Gaussian the confidence intervals are also obtained in regular fashion. We used 95% confidence intervals.

c. Calculating moments

The moments of the population distribution equilibrate after an initial phase dominated by the few initial cells in the population; see Fig. 4(a). Denoting by M_i the instantaneous value of a particular moment M (e.g., $\langle T\rangle$ or $\langle D^2\rangle$) at the discrete simulation output time t_i^s, we take the mean instantaneous simulated value upon equilibration for the simulated value of the moment,

$$M = \overline{M} = \frac{1}{\sum_{i>i^*} 1}\sum_{i>i^*} M_i, \tag{C3}$$

where i^* indicates onset of equilibration (taken to be $i^* = \frac{2}{3}N_{\mathrm{gens}}t_{\mathrm{min}}$). The standard error of the moment is obtained from the simulations using the same part of the simulated output,

$$\mathrm{SE}_M = \frac{1}{-2+\sum_{i>i^*} 1}\sum_{i>i^*}(M_i - \overline{M})^2. \tag{C4}$$

d. Calculating benefits B_D, B_T

The benefits, defined in Eq. (7) as $B_D = 1 - \frac{\langle D(a,\xi)\rangle}{\langle D(a=0,\xi=0)\rangle}$, $B_T = 1 - \frac{\langle T(a,\xi)\rangle}{\langle T(a=0,\xi=0)\rangle}$, describe the gain to the population from noise and/or ADS. The benefits are calculated from these definitions using the estimates of the population averages described above. Note that benefits cannot be computed from a single simulation in isolation, but are comparing across repeat simulations. The error of the benefits are obtained using error propagation and relying on the standard errors of the means of the statistical moments for $\langle T\rangle$ and $\langle D\rangle$ under the different values of a, ξ. Statistical significance of increase in benefit [Figs. 3(d) and 3(e)] was calculated using two-sample t-tests of full distributions from accepted cells (equilibrated population).

3. Adding cell-size control to simulations

To evaluate the impact of cell-size control (Appendix D), we reformulated the doubling time to depend on "sizer" division rules:

$$T = \frac{1}{\gamma}\ln\left(\frac{l_d}{l_{\mathrm{b}}}\right) + \eta, \tag{C5}$$

[29]. Here, T is the cell doubling time, γ is the single-cell growth rate, l_d (l_{b}) is the cell length at division (birth) and η is time-additive noise. Here we approximated cells to be rods with a constant radius.

The length $l^i(t)$ of cell i grows exponentially in time,

$$l^i(t) = l^i_{\mathrm{b}}\, e^{\gamma_i t}, \tag{C6}$$

where $\gamma_i = \ln 2/T_i^{\mathrm{ADS}}(n)$ is given by Eq. (2) for cell i in generation n. For the "adder" rule, a constant additional cell length Δl is assumed to be added before division. For the "sizer," all cells are assumed to grow to the same length l_{final} before dividing. The respective expressions for the doubling times are

$$T_i^{\mathrm{full,adder}} = \frac{1}{\gamma}\ln\left(\frac{l^i_{\mathrm{b}} + \Delta l}{l^i_{\mathrm{b}}}\right),$$
$$T_i^{\mathrm{full,sizer}} = \frac{1}{\gamma}\ln\left(\frac{l_{\mathrm{final}}}{l^i_{\mathrm{b}}}\right). \tag{C7}$$

Each simulation is started from a single cell, with the initial length drawn from a normal distribution with mean 1 μm and standard deviation 0.25 μm.

We have probed dividing the length in half both deterministically and stochastically [with $l_{\mathrm{offspring}} = c\, l_{\mathrm{mother}}$ and $(1-c)\, l_{\mathrm{mother}}$ and $c = 1/\nu$, $\nu \sim \mathcal{N}(2, 0.25)$].

APPENDIX D: NUMERICAL VERIFICATION THAT CELL-SIZE CONTROL AND DAMAGE-INDUCED DECREASE IN SINGLE-CELL GROWTH RATE ARE COMPATIBLE

It could be hypothesized that size-control mechanisms through their impact of cell lifetime [29], may dominate ADS effects on doubling time. Our results (Fig. 5) suggest that the size-control has very little impact on the population-level benefits from ADS.

The simulations in Fig. 5 are performed according to (Appendix C). For illustration, we introduce ΔT between the pure ADS and full (those including size-control) lifetimes,

$$\Delta T = T^{\mathrm{ADS}} - T, \tag{D1}$$

where T is given by Eq. (C5). Furthermore, we have also explored the impact of stochasticity in cell length at division by allowing for other than 50% split of mother cell length. No explicit time-additive noise was added to cell lifetimes [i.e., $\eta = 0$ in Eq. (C5)].

The reason that the size control has little effect on ADS benefits is as follows. Cells with more damage do take longer to divide, but their lengths will not vary from faster-growing cells because the growth of the cell's length is also slower. Because of this, cells with more damage do take longer to divide, but their lengths will not vary from faster-growing cells.

Our model retrieves the "timer" model if we do not explicitly model cell-size control.

APPENDIX E: POPULATION GROWTH AND NORMALIZED ENTROPY FROM NOISE AND ASYMMETRIC DAMAGE SEGREGATION VIA THE EULER–LOTKA APPROACH

1. Euler–Lotka model and method of cumulant expansion

The starting point for these analyses is the Euler–Lotka equation [46], which describes the growth of a population of dividing individuals in terms of the number of births $B(t)$ as a

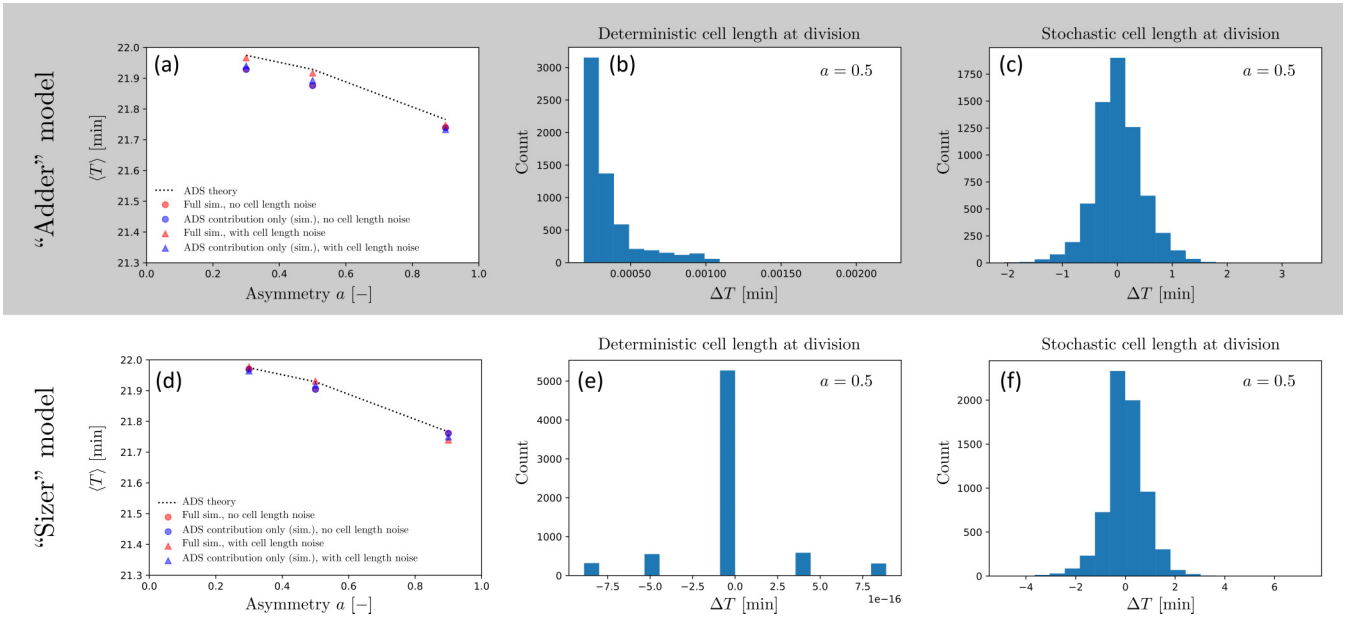

FIG. 5. Adding cell-size control to the system does not influence the conclusions of this study. For either model, the decrease in $\langle T \rangle$ (a), (d) predicted theoretically (dashed line) is still found both with (circles) or without (triangles) stochasticity in cell length at division. There is also little difference between the average pure ADS lifetime ($T^{\mathrm{ADS}} = \ln 2/\gamma$, blue) and the full average single-cell lifetime [including effects of ADS as well as cell-size control and given by Eq. (C5), red] for all studied cases. Examples of distributions of ΔT, the variations between pure ADS lifetimes and full single-cell lifetimes, have also been included for $a = 0.5$ (b), (c), (e), (f). These illustrate that the difference ΔT between the full single-cell lifetime and the pure ADS lifetime [see Eq. (D1)] is very small when cells divide deterministically exactly at the middle (panels **B** and **E**) because cell-size control ensures that any variations in cell length are quickly made negligible over few generations. However, the variations are noticeable when the cells divide stochastically (c), (f), but these are evenly distributed around the ADS lifetime, so these also do not impact the average population behavior because their contributions average to 0. Results calculated with $\lambda = 2, t_{\mathrm{min}} = 18$ min, $\mu = 1, N_{\mathrm{gens}} = 20$ and interrogated in a 20 min interval starting at 290 min; the first cell in the population has a random cell length drawn from a normal distribution with mean 1 μm and standard deviation of 0.25 μm, for "sizer" the cells divide when the reach a length of 3 μm and for "adder" they divide after adding 2 μm to their length at birth.

function of time t,

$$B(t) = \int_0^\infty B(t-\tau) g(\tau) b(\tau)\, d\tau, \tag{E1}$$

where $g(\tau)$ is the distribution of doubling times in the population and $b(\tau)$ specifies the reproductive rate for cells present at age τ. This equation holds independently of the mechanisms leading to the doubling-time and reproductivity distributions, i.e., it holds for both deterministic and stochastic cases. It is rewritten assuming exponential population growth $B(t) = N_0 \mathrm{e}^{Gt}$ where N_0 is a constant and G is the population growth rate, and furthermore assuming that any dividing cell produces two offsprint [$b(\tau) = 2$],

$$-\ln 2 = \ln \int_0^\infty e^{-G\tau} g(\tau)\, d\tau. \tag{E2}$$

The right-hand side is the cumulant-generating function for the random variable τ, a statistical function for which the coefficients of its Taylor-expansion are the statistical cumulants of the generation specified by $g(\tau)$ [59]. Assuming that the population growth G rate is small, we rewrite Eq. (E2) by truncating the Taylor series after the second-order term as

$$\ln 2 \approx \kappa_1 G - \tfrac{1}{2}\kappa_2 G^2, \tag{E3}$$

where κ_n is the nth cumulant of the distribution of doubling times $g(\tau)$ [50]. The first two cumulants κ_1, κ_2 correspond to the mean and variance, respectively. Using the method of series inversion we express G uniquely as a series expansion in terms of $\ln 2/\kappa_1$ [49,50],

$$G = \frac{\ln 2}{\kappa_1} + \varrho \left(\frac{\ln 2}{\kappa_1}\right)^2, \quad \varrho = \frac{1}{2}\frac{\kappa_2}{\kappa_1}. \tag{E4}$$

We show in Sec. S3 in the Supplemental Material [44] that the error from these approximations is on the order of a few percent for realistic conditions.

2. Population growth from noise alone

In the absence of asymmetry, all cells in the population grow at the same rate due to ADS, and any variation between single-cell doubling times is attributed to noise. We used this when we extracted the noise distribution from the experimental data, and so this noise distribution has zero mean. We take the population-mean single-cell doubling time to be given by ADS with $a = 0$ [Eq. (B12)] and use the variance σ_ξ^2 from the noise distribution in the following.

Invoking $\kappa_1 = \langle T(a=0) \rangle$ and $\kappa_2 = \sigma_\xi^2$ and solving Eq. (E3) for the population growth rate G yields the

population growth rate from noise,

$$G_\xi = \frac{\langle T(a=0)\rangle}{\sigma_\xi^2}\left[1-\sqrt{1-2\ln 2\frac{\sigma_\xi^2}{\langle T(a=0)\rangle^2}}\right]. \quad \text{(E5)}$$

a. Scaling noise with stress using constant coefficient of variation for noise

Using the assumption that the coefficient of variation for noise $C_V = \sigma_\xi/\langle T\rangle$ is conserved with C_V taken to be 0.23 (see Sec. II D), we include this in Eq. (E5) and together with the expression for $\langle T(a=0)\rangle$ from Eq. (B12) find

$$G_\xi = \frac{1}{C_V^2(t_{\min}+2\mu\lambda)}\left[1-\sqrt{1-2\ln 2\,C_V^2}\right]. \quad \text{(E6)}$$

An interesting observation from this expression is that the population grows slower under larger stress λ even though the standard deviation of the noise σ_ξ grows proportional to the stress. This explains why the population growth under noise alone decreases at large stress.

b. Population growth rate gain from noise alone

With the expression Eq. (E6) for the population growth rate G_ξ from the noise itself we obtain the growth rate gain from noise alone by subtracting the baseline growth rate of a population with ADS at $a=0$ [see also Eq. (7)],

$$\Delta G_\xi = G_\xi - G_{\rm ADS}(a=0). \quad \text{(E7)}$$

From Eq. (E6) with Eq. (B13) for $G_{\rm ADS}(a=0)$ we find

$$\Delta G_\xi = \frac{1}{C_V^2(t_{\min}+2\mu\lambda)}\left[1-\ln 2\,C_V^2-\sqrt{1-2\ln 2\,C_V^2}\right]. \quad \text{(E8)}$$

It follows from this expression that the entropy increase becomes smaller with stress, even as the noise amplitude grows proportional to the increase in average single-cell doubling time imposed by noise. This expression has been used in Fig. 3(c).

3. Population growth and entropy increase from ADS and noise together

To describe the population growth under both ADS and noise we return to Eq. (E1), which becomes

$$\frac{1}{2} = \int_0^\infty\int_{-\infty}^\infty e^{-G(\tau+\tau_\xi)} f_{\rm full}(\tau,\tau_\xi)\,d\tau_\xi\,d\tau, \quad \text{(E9)}$$

where $f_{\rm full}(\tau,\tau_\xi)$ is the joint probability distribution for ADS (τ) and noise (τ_ξ). Since ADS and noise are statistically independent (see Sec. II A), we can rewrite the right-hand side as $\int_0^\infty e^{-G\tau} f_{\rm ADS}(\tau)\,d\tau \int_{-\infty}^\infty e^{-G\tau_\xi} f_\xi(\tau_\xi) 2\,d\tau_\xi$ where $f_{\rm ADS}$ is the distribution of doubling times from ADS and f_ξ is the zero-mean distribution of noise. Upon taking the logarithm we find that the cumulant-generating functions for the contributions from ADS and noise separate

$$\ln\left(\int_0^\infty\int_{-\infty}^\infty e^{-G(\tau+\tau_\xi)} f_{\rm ADS}(\tau) f_\xi(\tau_\xi)\,d\tau_\xi\,d\tau\right) = \underbrace{\ln\int_0^\infty e^{-G\tau} f_{\rm ADS}(\tau)\,d\tau}_{\text{Contribution from ADS alone}} + \underbrace{\ln\int_{-\infty}^\infty e^{-G\tau_\xi} f_\xi(\tau_\xi)\,d\tau_\xi}_{\text{Contribution from noise alone}}. \quad \text{(E10)}$$

a. Solution from cumulant expansion

Each of the two terms in Eq. (E10) can be expanded in their cumulants [see Eq. (E3)], resulting in

$$\ln 2 \approx G_{\rm full}\langle T\rangle_{\rm ADS} - \frac{G_{\rm full}^2}{2}\left(\sigma_{\rm ADS}^2+\sigma_\xi^2\right), \quad \text{(E11)}$$

in which it has been used that the first cumulant is the mean and the second cumulant is the variance, and where it has been used that the mean damage is 0, $\langle T\rangle_\xi = 0$. Applying series inversion [Eq. (E4)] to this expression results in

$$G_{\rm full} \approx \frac{\ln 2}{\langle T\rangle_{\rm ADS}(a,\mu,\lambda,t_{\min})} + \frac{1}{2}\left[\frac{\sigma_{T,\rm ADS}^2(a,\mu,\lambda,t_{\min})}{\langle T\rangle_{\rm ADS}(a,\mu,\lambda,t_{\min})} + C_V^2\langle T\rangle_{\rm ADS}(a,\mu,\lambda,t_{\min})\right] \times\left(\frac{\ln 2}{\langle T\rangle_{\rm ADS}(a,\mu,\lambda,t_{\min})}\right)^2, \quad \text{(E12)}$$

where $\langle T\rangle_{\rm ADS}$, $\sigma_{T,\rm ADS}^2$ are given by Eqs. (6) and (B6).

It is now straightforward to obtain an expression for the population growth rate gain ΔG by subtracting $G(a=0,\xi=0)$ from Eq. (E12),

$$\Delta G_{\rm full} \approx \frac{\ln 2}{\langle T\rangle_{\rm ADS}(a,\mu,\lambda,t_{\min})} + \frac{1}{2}\left[\frac{\sigma_{T,\rm ADS}^2(a,\mu,\lambda,t_{\min})}{\langle T\rangle_{\rm ADS}(a,\mu,\lambda,t_{\min})} + C_V^2\langle T\rangle_{\rm ADS}(a,\mu,\lambda,t_{\min})\right] \times\left(\frac{\ln 2}{\langle T\rangle_{\rm ADS}(a,\mu,\lambda,t_{\min})}\right)^2 - \frac{\ln 2}{t_{\min}+2\mu\lambda}, \quad \text{(E13)}$$

which is given in Eq. (7) and used in Fig. 3(c).

[1] M. Hashimoto, T. Nozoe, H. Nakaoka, R. Okura, S. Akiyoshi, K. Kaneko, E. Kussell, and Y. Wakamoto, Noise-driven growth rate gain in clonal cellular populations, Proc. Natl. Acad. Sci. USA **113**, 3251 (2016).

[2] A. J. Lee, S. Wang, H. R. Meredith, B. Zhuang, Z. Dai, and L. You, Robust, linear correlations between growth rates and β-lactam–mediated lysis rates, Proc. Natl. Acad. Sci. USA **115**, 4069 (2018).

[3] O. Gefen and N. Q. Balaban, The importance of being persistent: Heterogeneity of bacterial populations under antibiotic stress, FEMS Microbiol. Rev. **33**, 704 (2009).

[4] S. Vedel, S. Tay, D. M. Johnston, H. Bruus, and S. R. Quake, Migration of cells in a social context, Proc. Natl. Acad. Sci. USA **110**, 129 (2013).

[5] A. Eldar and M. B. Elowitz, Functional roles for noise in genetic circuits, Nature (London) **467**, 167 (2010).

[6] R. Pugatch, Greedy scheduling of cellular self-replication leads to optimal doubling times with a log-frechet distribution, Proc. Natl. Acad. Sci. USA **112**, 2611 (2015).

[7] D. A. F. Fuentes, P. Manfredi, U. Jenal, and M. Zampieri, Pareto optimality between growth-rate and lag-time couples metabolic noise to phenotypic heterogeneity in *Escherichia coli*, Nat. Commun. **12**, 3204 (2021).

[8] A. M. Proenca, C. U. Rang, C. Buetz, C. Shi, and L. Chao, Age structure landscapes emerge from the equilibrium between aging and rejuvenation in bacterial populations, Nat. Commun. **9**, 3722 (2018).

[9] J. Borgqvist, N. Welkenhuysen, and M. Cvijovic, Synergistic effects of repair, resilience and retention of damage determine the conditions for replicative ageing, Sci. Rep. **10**, 1556 (2020).

[10] E. J. Stewart, R. Madden, G. Paul, and F. Taddei, Aging and death in an organism that reproduces by morphologically symmetric division, PLoS Biol. **3**, e45 (2005).

[11] M. Coelho, A. Derelu, A. Haese, S. Kühn, L. Malinovska, M. E. DeSantis, J. Shorter, S. Alberti, T. Gross, and I. M. Tolić-Nørrelykke, Fission yeast does not age under favorable conditions, but does so after stress, Curr. Biol. **23**, 1844 (2013).

[12] N. Erjavec, M. Cvijovic, E. Klipp, and T. Nyström, Selective benefits of damage partitioning in unicellular systems and its effect on aging, Proc. Natl. Acad. Sci. USA **105**, 18764 (2008).

[13] L. Chao, A model for damage load and its implications for the evolution of bacterial aging, PLoS Genet. **6**, e1001076 (2010).

[14] J. Winkler, A. Seybert, L. König, S. Pruggnaller, U. Haselmann, V. Sourjik, M. Weiss, A. S. Frangakis, A. Mogk, and B. Bukau, Quantitative and spatio-temporal features of protein aggregation in *Escherichia coli* and consequences on protein quality control and cellular ageing, EMBO J. **29**, 910 (2010).

[15] A. B. Lindner, R. Madden, A. Demarez, E. J. Stewart, and F. Taddei, Asymmetric segregation of protein aggregates is associated with cellular aging and rejuvenation, Proc. Natl. Acad. Sci. USA **105**, 3076 (2008).

[16] S. Vedel, H. Nunns, A. Košmrlj, S. Semsey, and A. Trusina, Asymmetric damage segregation constitutes an emergent population-level stress response, Cell Syst. **3**, 187 (2016).

[17] M. Ackermann, L. Chao, C. T. Bergstrom, and M. Doebeli, On the evolutionary origin of aging, Aging Cell **6**, 235 (2007).

[18] R. Z. Moger-Reischer and J. T. Lennon, Microbial ageing and longevity, Nat. Rev. Microbiol. **17**, 679 (2019).

[19] M. Ogrodnik, H. Salmonowicz, and V. N. Gladyshev, Integrating cellular senescence with the concept of damage accumulation in aging: Relevance for clearance of senescent cells, Aging Cell **18**, e12841 (2019).

[20] T. Nyström, A bacterial kind of aging, PLoS Genet **3**, e224 (2007).

[21] M. Ogrodnik, H. Salmonowicz, R. Brown, J. Turkowska, W. Sredniawa, S. Pattabiraman, T. Amen, A.-c. Abraham, N. Eichler, R. Lyakhovetsky, and D. Kaganovich, Dynamic junq inclusion bodies are asymmetrically inherited in mammalian cell lines through the asymmetric partitioning of vimentin, Proc. Natl. Acad. Sci. USA **111**, 8049 (2014).

[22] Y. Miyazaki, K. Mizumoto, G. Dey, T. Kudo, J. Perrino, L.-c. Chen, T. Meyer, and T. J. Wandless, A method to rapidly create protein aggregates in living cells, Nat. Commun. **7**, 11689 (2016).

[23] M. R. Bufalino, B. DeVeale, and D. van der Kooy, The asymmetric segregation of damaged proteins is stem cell-type dependent, J. Cell Biol. **201**, 523 (2013).

[24] M. A. Rujano, F. Bosveld, F. A. Salomons, F. Dijk, M. A. van Waarde, J. J. van der Want, R. A. de Vos, E. R. Brunt, O. C. Sibon, and H. H. Kampinga, Polarised asymmetric inheritance of accumulted protein damage in higher eukaryotes, PLoS Biol. **4**, e417 (2006).

[25] D. L. Moore, G. A. Pilz, M. J. Araúzo-Bravo, Y. Barral, and S. Jessberger, A mechanism for the segregation of age in mammalian neural stem cells, Science **349**, 1334 (2015).

[26] E. Ising, Beitrag zur theorie des ferromagnetismus, Z. Phys. **31**, 253 (1925).

[27] J. M. Yeomans, *Statistical Mechanics of Phase Transitions* (Oxford University Press, Oxford, UK, 1992).

[28] O. Patange, C. Schwall, M. Jones, C. Villava, D. A. Griffith, A. Phillips, and J. C. W. Locke, *Escherichia coli* can survive stress by noisy growth modulation, Nat. Commun. **9**, 5333 (2018).

[29] J. Lin and A. Amir, The effects of stochasticity at the single-cell level and cell size control on the population growth, Cell Syst. **5**, 358 (2017).

[30] I. Soifer, L. Robert, and A. Amir, Single-cell analysis of growth in budding yeast and bacteria reveals a common size regulation strategy, Curr. Biol. **26**, 356 (2016).

[31] S. Taheri-Araghi, S. Bradde, J. T. Sauls, N. S. Hill, P. A. Levin, J. Paulsson, M. Vergassola, and S. Jun, Cell-size control and homeostasis in bacteria, Curr. Biol. **25**, 385 (2015).

[32] M. Campos, I. V. Surovtsev, S. Kato, A. Paintdakhi, B. Beltran, S. E. Ebmeier, and C. Jacobs-Wagner, A constant size extension drives bacterial cell size homeostasis, Cell **159**, 1433 (2014).

[33] C. Nieto, J. Arias-Castro, C. Sánchez, C. Vargas-García, and J. M. Pedraza, Unification of cell division control strategies through continuous rate models, Phys. Rev. E **101**, 022401 (2020).

[34] S. Leibler and E. Kussell, Individual histories and selection in heterogeneous populations, Proc. Natl. Acad. Sci. USA **107**, 13183 (2010).

[35] E. Kussell and S. Leibler, Phenotypic diversity, population growth, and information in fluctuating environments, Science **309**, 2075 (2005).

[36] Y. Wakamoto, A. Y. Grosberg, and E. Kussell, Optimal lineage principle for age-structured populations, Evolution **66**, 115 (2012).

[37] A. Amir, Cell size regulation in bacteria, Phys. Rev. Lett. **112**, 208102 (2014).

[38] A. Marantan and A. Amir, Stochastic modeling of cell growth with symmetric and asymmetric division, Phys. Rev. E **94**, 012405 (2016).

[39] J. Lin and A. Amir, From single-cell variability to population growth, Phys. Rev. E **101**, 012401 (2020).

[40] J. Lin, J. Min, and A. Amir, Optimal segregation of proteins: Phase transitions and symmetry breaking, Phys. Rev. Lett. **122**, 068101 (2019).

[41] J. Min and A. Amir, A transport approach to relate asymmetric protein segregation and population growth, J. Stat. Mech. (2021) 073503.

[42] B. K. Kennedy, N. R. Austriaco, Jr, and L. Guarente, Daughter cells of *Saccharomyces cerevisiae* from old mothers display a reduced life span, J. Cell Biol. **127**, 1985 (1994).

[43] J.-W. Veening, E. J. Stewart, T. W. Berngruber, F. Taddei, O. P. Kuipers, and L. W. Hamoen, Bet-hedging and epigenetic inheritance in bacterial cell development, Proc. Natl. Acad. Sci. USA **105**, 4393 (2008).

[44] See Supplemental Material at http://link.aps.org/supplemental/10.1103/PhysRevE.109.054404 for more details.

[45] N. N. Taleb, *Antifragile: Things That Gain from Disorder* (Random House, New York, NY, 2012).

[46] B. Charlesworth, Fisher, Medawar, Hamilton and the evolution of aging, Genetics **156**, 927 (2000).

[47] E. Levien, J. Kondev, and A. Amir, The interplay of phenotypic variability and fitness in finite microbial populations, J. R. Soc. Interface **17**, 20190827 (2020).

[48] E. Levien, T. GrandPre, and A. Amir, Large deviation principle linking lineage statistics to fitness in microbial populations, Phys. Rev. Lett. **125**, 048102 (2020).

[49] M. Abramowitz and I. Stegun, *Handbook of Mathematical Functions with Formulas, Graphs, and Mathematical Tables* (Dover Publications, 1965).

[50] S. Schindler, S. Tuljapurkar, J.-M. Gaillard, and T. Coulson, Linking the population growth rate and the age-at-death distribution, Theor. Popul. Biol. **82**, 244 (2012).

[51] L. S. Tsimring, Noise in biology, Rep. Prog. Phys. **77**, 026601 (2014).

[52] R. H. Chisholm, T. Lorenzi, A. Lorz, A. K. Larsen, L. N. de Almeida, A. Escargueil, and J. Clairambault, Emergence of drug tolerance in cancer cell populations: An evolutionary outcome of selection, nongenetic instability, and stress-induced adaptation, Cancer Res. **75**, 930 (2015).

[53] A. Brauner, O. Fridman, O. Gefen, and N. Q. Balaban, Distinguishing between resistance, tolerance and persistence to antibiotic treatment, Nat. Rev. Microbiol. **14**, 320 (2016).

[54] N. Q. Balaban, S. Helaine, K. Lewis, M. Ackermann, B. Aldridge, D. I. Andersson, M. P. Brynildsen, D. Bumann, A. Camilli, J. J. Collins *et al.*, Definitions and guidelines for research on antibiotic persistence, Nat. Rev. Microbiol. **17**, 441 (2019).

[55] T. Bergmiller, A. M. Andersson, K. Tomasek, E. Balleza, D. J. Kiviet, R. Hauschild, G. Tkačik, and C. C. Guet, Biased partitioning of the multidrug efflux pump AcrAB-TolC underlies long-lived phenotypic heterogeneity, Science **356**, 311 (2017).

[56] S. K. Govers, J. Mortier, A. Adam, and A. Aertsen, Protein aggregates encode epigenetic memory of stressful encounters in individual *Escherichia coli* cells, PLoS Biol. **16**, e2003853 (2018).

[57] T. S. Ursell, J. Nguyen, R. D. Monds, A. Colavin, G. Billings, N. Ouzounov, Z. Gitai, J. W. Shaevitz, and K. C. Huang, Rod-like bacterial shape is maintained by feedback between cell curvature and cytoskeletal localization, Proc. Natl. Acad. Sci. USA **111**, E1025 (2014).

[58] L. Wasserman, *All of Statistics—A Concise Course in Statistical Inference* (Springer, Berlin, 2004).

[59] N. G. van Kampen, *Stochastic Processes in Physics and Chemistry*, 3rd ed. (North-Holland Personal Library, Amsterdam, 2007).